Journal of Hazardous Materials 459 (2023) 132162

Contents lists available at ScienceDirect

Journal of Hazardous Materials

journal homepage: www.elsevier.com/locate/jhazmat

Typical heavy metals accumulation, transport and allocation in a deglaciated forest chronosequence, Qinghai-Tibet Plateau

Peijia Chen [a], Xun Wang [b], Wei Yuan [b], Dingyong Wang [a,*]

[a] College of Resources and Environment, Southwest University, Chongqing 400715, China
[b] State Key Laboratory of Environmental Geochemistry, Institute of Geochemistry, Chinese Academy of Sciences, Guiyang 550081, China

HIGHLIGHTS

- Atmospheric deposition likely dominants the major source of Hg in topsoil.
- Moraine weathering likely as the main source of Cr in topsoil.
- The main source of Cd shifted from moraine weathering to atmospheric depositions.
- Vegetation succession shapes the accumulation of Hg, Cd and Cr in the glacial retreat area.

GRAPHICAL ABSTRACT

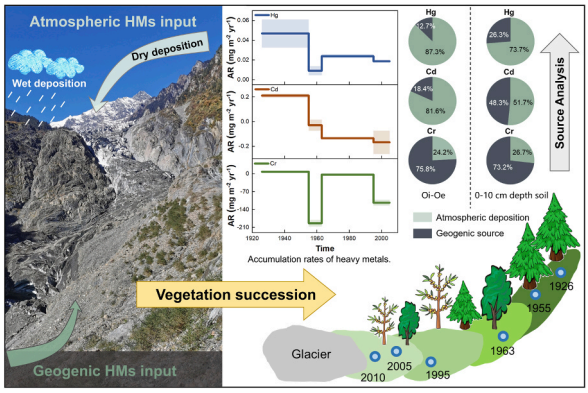

ARTICLE INFO

Editor: Joao Pinto da Costa

Keywords:
Qinghai-Tibet Plateau
Glacial retreat area
Vegetation succession
Mercury
Cadmium
Chromium
Source analysis

ABSTRACT

Understanding heavy metals (HMs) accumulation and transportation is the foundation to assess the ecological risks caused by the pollution of HMs in terrestrial ecosystems. There are large knowledge gaps regarding impacts of vegetation succession on shaping the HMs accumulation, transportation and allocation in the remote alpine regions. Herein, we comprehensively investigated the distribution and source contribution of mercury (Hg), cadmium (Cd) and chromium (Cr) along with vegetation succession in a deglaciated forest chronosequence of Qinghai-Tibet Plateau. Results showed that Hg and Cd were highly enriched in organic soils, while Cr concentrations and pool sizes decreased significantly with the vegetation succession. Atmospheric Hg deposition contributed to the dominant Hg sources in topsoil (74 – 87%), whereas moraine weathering was the main source of Cr (73 – 76%). Both moraine (18 – 48%) and atmospheric deposition inputs (52 – 82%) affected Cd accumulation in topsoil. Over the last century, the accumulation rate of Hg and Cd showed the distinctly decreasing trends due to the vegetation leading to the elevated atmospheric depositions at the earlier deglacial sites. The negative accumulation rate of Cr along with the vegetation succession reflected the formation of organic soil diluting the geogenic inputs of Cr.

* Corresponding author.
E-mail address: dywang@swu.edu.cn (D. Wang).

https://doi.org/10.1016/j.jhazmat.2023.132162
Received 26 May 2023; Received in revised form 25 July 2023; Accepted 25 July 2023
Available online 26 July 2023

1. Introduction

Mercury (Hg), cadmium (Cd) and chromium (Cr) are well-known toxic elements and threat to human health because of their high toxicity and biomagnification [19,31]. Currently, Hg, Cd and Cr have been listed as priority pollutants for monitoring and controlling in many countries and regions [20,51]. The increasing anthropogenic emissions since the Industrial Revolution have greatly increased the amount of Hg, Cd and Cr in the environment, thus distinctly having disturbed their naturally biogeochemical cycles in the alpine ecosystems [91,59,61,88]. More than 95% of Hg in the atmosphere is as the elemental Hg vapor (Hg^0), which has a residence time of approximately 0.3 – 1.5 years [52, 66,76,92]. Cd and Cr tend to transport in the form of fine particulates in the air, and remain in the atmosphere for several days to weeks [81,83]. The atmospheric wet and dry depositions of Hg, Cd and Cr in the remote alpine regions lead to the remarked increase of their concentrations compared to previously existed only in much smaller quantities of natural origins [9,26,44,86,99].

Substantial studies have demonstrated the distribution, sources and ecological risk of heavy metals (HMs) accumulation in alpine ecosystems [100,119,16,27,29,42,56,7,8]. HMs accumulation in the alpine ecosystem is affected by various input sources (e.g., atmospheric depositions, mineral weathering), environmental conditions (e.g., precipitation, temperature and vegetation), soil chemical properties (e.g., soil organic matter and pH) and microorganisms [32,35,41,60]. Specifically, vegetation plays an important role in shaping the spatial distribution of HMs, by influencing the rate of HMs depositions, enhancing the rock weathering processes due to complicated impacts of root, and improving soil organic matter complexion with HMs [96,21]. Nevertheless, the field sampling and observations mainly focused on the spatial distribution and depositions of HMs, yet the temporal trends of HMs accumulation, transportation and allocation among the interface of air-vegetation-soil are not well understood.

Global warming accelerates the shrinking of alpine glaciers since the Little Ice Age [10,108]. The glacial retreated region with 1 – 2 km distance basically has the almost similar climatic and geographical conditions. The intensive ice-layer blocks the atmospheric deposition into the underlayer soil, while after the glacier retreated, the underlayer soil begins to accumulate the atmospheric depositions [97,98]. Recent studies highlight that glacier-to-vegetation succession in the deglaciated region provides a unique opportunity to study the sources and sequestration of HMs over time in alpine ecosystems [109,94,98,93].

Therefore, we aimed to comprehensively understand the accumulation, transportation and different source contribution of Hg, Cd and Cr along with vegetation succession in a deglaciated forest chronosequence of Qinghai-Tibet Plateau. In this study, we applied the data describing variations of HMs in a deglaciated forest chronosequence to illustrate the effects of vegetation change on the biogeochemical processes of HMs. Correlation analysis, enrichment factors, and Positive Matrix Factorization (PMF) model were applied to quantify source contributions and to assess impacts of the important factors on affecting the allocation of Hg, Cd and Cr among the interface of air-soil-vegetation. Finally, the accumulation rates were further estimated to understand the transport and accumulation of HMs along with vegetation succession over last century.

2. Materials and methods

2.1. Study area and sampling sites

Mingyong Glacier is located in the southeastern Qinghai-Tibet Plateau, and as one of the major glacier systems on the eastern slope of Meri Snow Mountain (98°45′ E, 28°27′ N, peak elevation: 6740 m a. s. l.). The global warming since the 1930 s has accelerated the retreat of Mingyong Glacier (Yuanqing et al., 2008; [118]). The local geomorphological environment has changed rapidly due to the glacial retreat, and a complete primary forest chronosequence covering a distance of ~ 2 km has established at the elevation of 2518 – 2779 m. The vegetation in the deglaciated forest chronosequence varies from the pioneer species of sea-buckthorn (*Hippophae rhamnoides* Linn.) and aspen (*Populus rotundifolia var. bonati (Levl.)* C. Wang et Tung) to the climax community of fir (*Abies fabri (Mast.)* Craib). The climate over the deglaciated forest chronosequence is characterized as the relatively low temperature with an annual average ranging from – 2–2 °C. The annual mean precipitation is 600 – 700 mm [113,114].

We set six sampling sites along with the deglaciated forest chronosequence (Fig. 1). The glacier retreated time at each site has been well documented in our earlier study [98]. Briefly, the glacier retreated time was determined by the time interval between the settlement of pioneer species in the bare land (i.e., the time between glacial retreat and sapling germination) and the maximum age of trees at each site in the glacial retreat area. The glacier retreated time at our selected six sampling sites is the year of 2010, 2005, 1995, 1963, 1955 and 1926. The sea-buckthorn and aspen are the dominant tree species at sites glacier retreated of 1995–2010. The mixed forests dominated by sea-buckthorn, aspen and fir developed at sites representing the retreat between 1955 and 1963. The stable and mature climax community of fir forest has developed at sites of retreat before 1926.

2.2. Sample collection

During autumn of 2019 – 2022, we comprehensively collected soil and vegetation samples at six sites in the deglaciated forest chronosequence. Three 0.5 m × 0.5 m subplots at each site were established to collect soil profile samples. Due to the difference in plant productivity, the thickness of the organic soil layer ranges from 1 to 10 cm depending on the glacial treated time. At all sites, the soil profile is divided into Oi (slightly decomposed litter), Oe (mo the derately decomposed litter),0- to 5-, 5- to 10- cm and deep C (soil parent horizon) soil horizons. It is noted that the Oe horizon has been not well formed at the 1995–2005 sites due to the short time of vegetation succession. The soil below the Oe horizon was collected by a steel auger drill (5 cm diameter). To avoid the influence of surface soil, we collected soil samples at the 40 cm depth of soil profile as the deep C soil.

For vegetation sampling, 5 – 7 tree cores were drilled at the breast

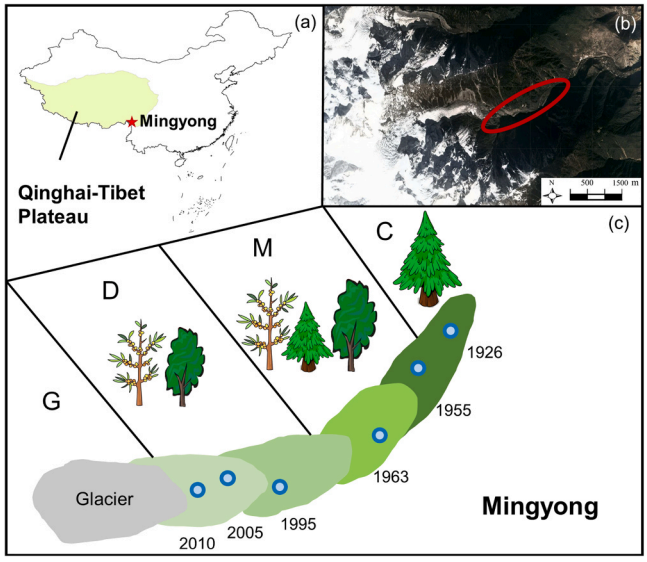

Fig. 1. Sampling sites in a forest chronosequence zone at deglaciated terrain of Mingyong. (a) the location of Mingyong Glacier in China; (b) satellite imagery of Mingyong Glacier; (c) land cover types in Mingyong Glacier. G indicates the glacier, D is the deciduous forest, M is the mixed forest and C is the coniferous forest.

height (1.3 m) of trees at each site by using an increment borer (Haglof, diameter 5 mm). Meanwhile, we sampled 200 − 500 g biomass of foliage, branch, bark and root from each drilled tree. In total, 243 vegetation and 156 soil samples were collected. Samples were transported to the laboratory and oven-dried (at 45 ℃) to a constant mass (the mass difference between two 8- hour heating < 0.03%). The dried samples were ground by an agate grinder and sieved with a 200–mesh (74 μm) sieve, and the fraction passed through the sieve was placed in metal-free plastic bags for chemical analysis.

2.3. Chemical analysis

The Hg concentrations in vegetation and soil samples were measured on a DMA80 Hg analyzer, following the protocol described in our earlier studies [97,95]. Soil organic matter (SOM) content was determined by the Walkley-Back method which involves oxidation of SOM by $Cr_2O_7^{2-}$ followed by the addition of $FeSO_4$ to reduce the excess $Cr_2O_7^{2-}$ [89]. The Cd and Cr concentrations were analyzed by Inductively Coupled Plasma Mass Spectrometry (ICP-MS, Agilent - 7900) following the procedures of USA EPA Method 6020B. Briefly, about 0.1 g soil samples were digested in a closed Teflon vessel by an acid mixture (HNO_3:HF = 5:1, v/v) at 150 ºC for 48 h. The digested solution was transferred quantitatively with ultra-pure water to a 50 mL Teflon bottle and analyzed by ICP-MS. Additionally, we also measured arsenic (As), lead (Pb), lithium (Li), beryllium (Be), vanadium (V), manganese (Mn), cobalt (Co), nickel (Ni), zinc (Zn), gallium (Ga), rubidium (Rb), silver (Ag), strontium (Cs), barium (Ba), thallium (Tl) and uranium (U) concentrations in vegetation and soil samples by ICP-MS. These trace metals were used to build the Positive Matrix Factorization (PMF) model to estimate source contribution. The aluminum (Al) concentration was analyzed by Inductively Coupled Plasma Optical Emission Spectroscopy (ICP-OES).

2.4. Quality assurance and quality control (QA/QC)

The National Standard Reference Materials (SRM) of China GBW07405 (GSS-5, soil), GBW10020 (GSB-11, vegetation) and GBW10049 (GSB-27, vegetation) were used for quality assurance/quality control (QA/QC). For Hg measurement, the SRM were measured after every 9 samples with a recovery of 95 − 105%. For measuring other trace metals, the SRM, blank and replicated samples were analyzed in every 10 treatments (7 samples + 1 SRM + 1 blank + 1 replicated sample). The average percentages of measured trace element in the SRM yielded a recovery of 91 − 104%. The deviation of HM concentrations in replicated samples was less than 5%.

2.5. Estimation of enrichment factor and pool size

The enrichment factor (EF) for HMs was calculated to assess the accumulation of HMs in the soil [17,40]:

$$EF = \frac{(C/R)_{soil}}{(C/R)_{C\ layer}} \quad (1)$$

where C is the trace element concentration, and R is the reference element concentration of Al (Aluminum) in this study. This is because the Al in soil mainly deriving from the rock weathering processes, and the Al concentration in C soil shows no significant difference during the succession (Fig. S1; $p > 0.05$). To evaluate the degree of accumulation for Hg, Cd and Cr, the following accumulation gradations are proposed [1]: EF< 1, no / low accumulation; 1 ≤ EF < 3, moderate; 3 ≤ EF < 6, considerable; 6 ≤ EF, very high accumulation. The bioconcentration factor (BCF) and the translocation factor (TF) are defined as the transferability of HMs from soil to plant [30]:

$$BCF = \frac{C_{root}}{C_{soil}} \quad (2)$$

$$TF = \frac{C_{aboveground}}{C_{root}} \quad (3)$$

where C_{root} and $C_{aboveground}$ are the concentration of HMs in the root and aboveground biomass of plants, respectively. C_{soil} represents the corresponding value in the soil. BCF> 1 indicates that heavy metal enhanced accumulation in roots [67]. TF> 1 means the aboveground biomass has a stronger ability to accumulate HMs than the root [112]. It is noted that BCF and TF are mainly applicable to HMs which uptake by root then translocation into the aboveground biomass.

Species-specific allometric equations (Table S1) were applied to estimate the variation of vegetation biomass density (Table S2) across the deglaciated forest chronosequence. The Hg, Cd and Cr pool sizes were estimated based on the measured soil bulk density (Table S3) and vegetation biomass density:

$$Pool_{soil} = \sum [Con_{soil} \times BulkDensity_{soil} \times Depth \times (1 - f)] \quad (4)$$

$$Pool_{veg} = \sum (Con_{veg} \times Biomass_{veg}) \quad (5)$$

where f is the soil coarse fragments (> 2 mm) volume ratio in surface soil.

2.6. Data analysis

The IBM SPSS Statistics v26.0 was used for statistical analysis at 95% confidence level. We used One-Way ANOVA to conduct the significant difference analysis when data were normally distributed. Otherwise, the Kruskal-Wallis test was applied. Pearson correlation analysis was applied to evaluate the relation between different variables. We also used EPA (Environmental Protection Agency) PMF (Positive Matrix Factorization) 5.0 to estimate the source contributions of atmospheric depositions and geogenic inputs for Hg, Cd and Cr. Table S4 showed the final results of model predictions by PMF. After 300-iteration, we obtained 3 factors, with the smallest Q value and residual ranging between − 3 and 3 in PMF. The coefficient between the observed value and predicted value (R^2) were greater than 0.66 for most HMs.

3. Results

3.1. Distribution of Hg, Cd and Cr in soil profiles

Fig. 2 (a−c) demonstrates variations of Hg, Cd and Cr concentrations along with deglaciated forest chronosequence. The soil Hg concentrations were comparable at sites of 1995 − 2005 ($p > 0.05$, one-way ANOVA), and so do Cd and Cr concentrations. The topsoil Hg concentrations (Oi, Oe and 0–10 cm depth) increased with the vegetation succession (2005 site: 33.90 ± 8.20 μg kg^{-1}; 1926 site: 94.99 ± 47.13 μg kg^{-1}). The mean Cd concentrations in topsoil showed the lowest value (0.27 ± 0.04 mg kg^{-1}) at 1963 site while the highest value (0.33 ± 0.17 mg kg^{-1}) at 1926 site. The mean Cr concentrations in topsoil decreased with glacial retreat time (2005 site: 71.46 ± 29.97 mg kg^{-1}; 1926 site: 42.13 ± 24.87 mg kg^{-1}). The mean Cd and Cr concentrations in C soil had the value of 0.35 ± 0.07 mg kg^{-1} and 91.15 ± 7.34 mg kg^{-1} across the forest chronosequence, respectively. The average Hg concentrations in topsoil were significantly higher than in C soil across the deglacial forest chronosequence, while Cr concentrations increased along with the increasing soil depth except for the 1963 site ($p < 0.05$).

Fig. 2 (d−f) exhibits correlations between soil Hg, Cd and Cr concentrations and SOM contents and Fig. 2 (g−i) shows correlations between soil Hg, Cd and Cr concentrations and pH. The soil Hg concentration showed a significantly positive correlation with SOM content ($R^2 = 0.84$, $p < 0.01$) and a significantly negative correlation with pH ($R^2 = 0.26$, $p < 0.01$). However, the soil Cr concentration had a significantly negative correlation with SOM content ($R^2 = 0.81$,

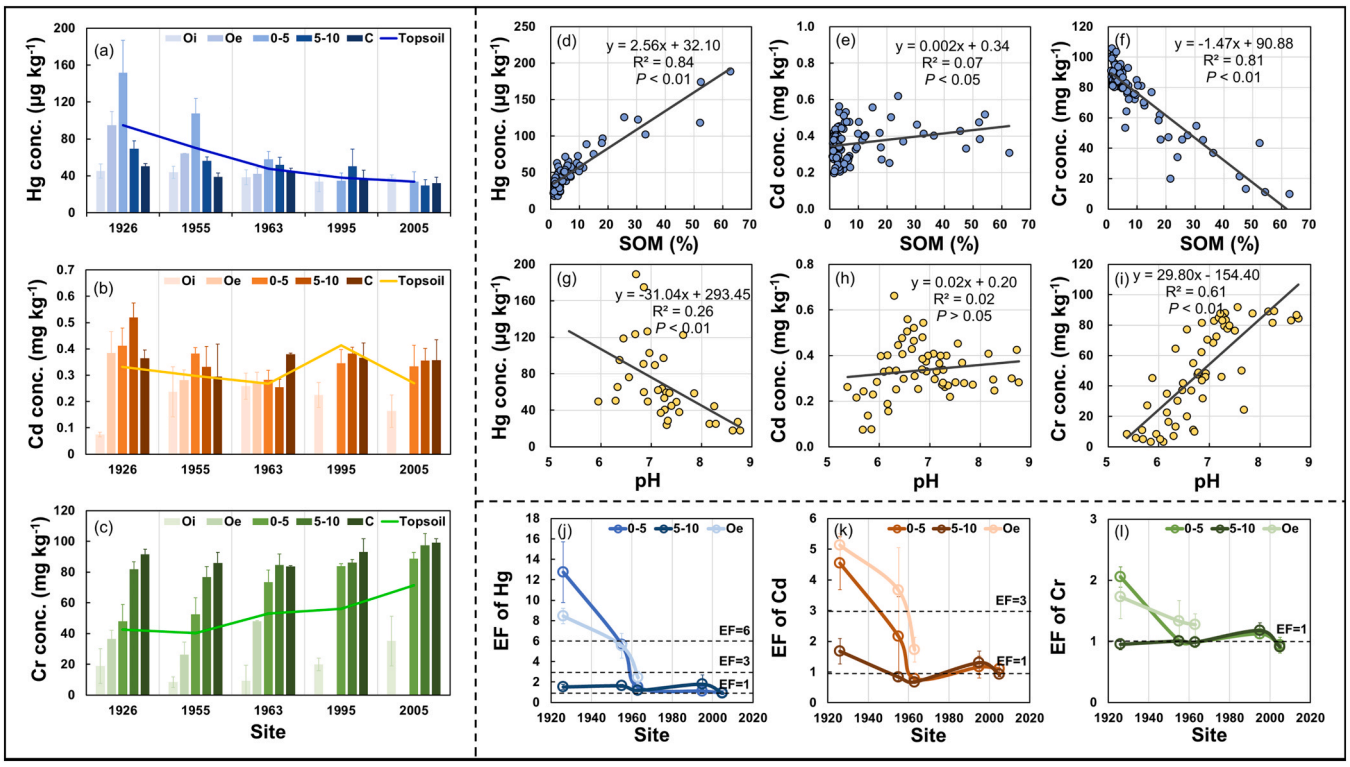

Fig. 2. Variations of Hg, Cd and Cr concentration (conc.) across the deglaciated forest chronosequence. (a-c) variations of Hg, Cd and Cr concentrations in soil in the deglaciated forest chronosequence; (d-i) correlations among soil Hg, Cd and Cr concentrations, SOM content and pH value; (j-l) variations of Hg, Cd and Cr enrichment factor (EF) in forest chronosequence zone.

$p < 0.01$) and a positive correlation with pH ($R^2 = 0.61$, $p < 0.01$). Insignificant correlations were observed between Cd and SOM ($R^2 = 0.07$, $p < 0.05$), and between Cd and pH ($R^2 = 0.02$, $p > 0.05$).

Fig. 2 (j – l) shows variations of EF for Hg, Cd and Cr across the deglaciated forest chronosequence. All EF values in Oe and 0–5 cm depth soils increased along with the vegetation succession. The short time (less than 60-year) of soil development leads to the similar soil properties and comparable Hg, Cd and Cr concentrations between in 0–10 cm depth soils and C layer, which resulted in the close to 1.0 values of EF. At the oldest deglacial forest site, Cd and Cr exhibited a moderate accumulation in Oe (EF of Cd: 5.12 ± 0.38; EF of Cr: 1.73 ± 0.36) and 0–5 cm depth soils (EF of Cd: 4.55 ± 0.86, EF of Cr: 2.05 ± 0.17), and Hg showed an extreme accumulation with an EF value of 13 in 0–5 cm depth soils.

3.2. Distribution of Hg, Cd and Cr in vegetation

Fig. 3 depicts variations of concentration, bioconcentration factor (BCF) and translocation factor (TF) for Hg, Cd and Cr in plants. The foliage of all tree species had the highest Hg concentration, specifically up to 17 times higher than in stem (foliage: 16.12 ± 7.59 μg kg^{-1}; stem: 0.97 ± 0.76 μg kg^{-1}). The Hg concentrations in foliage of the three tree species ranked as fir (26.19 ± 3.94 μg kg^{-1}) > sea-buckthorn (15.09 ± 2.42 μg kg^{-1}) > aspen (10.80 ± 7.71 μg kg^{-1}) ($p < 0.05$). For sea-buckthorn and aspen, roots had the second highest Hg concentration with values 1 – 15 times higher than those of bark, branches and stems. For fir, the Hg concentration of branches are 1 – 11 times higher than values in roots, bark and stems. For sea-buckthorn and fir, roots had the highest Cd concentrations with values 2 – 33 times higher than those of bark, branches and stems. However, Cd concentrations in bark, leaves and branches of aspen were 2 – 3 times higher than those in roots. Cr concentrations in roots of the three tree species were 3 – 31 times higher than in aboveground biomass.

The BCF values of Hg, Cd and Cr ranged 0.11 – 0.24, 0.13 – 0.68 and 0.10 – 0.37 for all tree species, respectively. The TF of Hg in foliage had the highest values for all three tree species, up to 4 – 20 times than TF values of other vegetation components (branches: 0.45 – 1.04; bark: 0.51 – 0.67; stem: 0.08 – 0.19). For Cd and Cr, the bark of sea buckthorn and aspen had the highest TF values (Cd: 0.27 ± 0.11 and 3.68 ± 1.67; Cr: 0.19 ± 0.17 and 0.24 ± 0.16, respectively), while branches of fir had the highest TF values (Cd: 0.50 ± 0.33; Cr: 0.60 ± 0. 46). Cd and Cr in stem of all three tree species had the lowest TF than other vegetation components (Cd: 0.03 – 0.79; Cr: 0.04 – 0.19).

3.3. Variations of Hg, Cd and Cr pool size along the glacier retreated area

Fig. 4 shows Hg, Cd and Cr pool sizes in vegetation and soil profiles. The Hg, Cd and Cr pool in stem, root, foliage and branch all increased along with the vegetation succession. The total vegetation pool sizes of Hg, Cd and Cr at 1926 site (Hg: 0.05 ± 0.01 mg m^{-2}; Cd: 0.57 ± 0.21 mg m^{-2}; Cr: 27.23 ± 3.47 mg m^{-2}) were 10, 11 and 5 times higher than values at 2010 site (Hg: 4.91 $\times 10^{-3}$ ± 1.26 $\times 10^{-3}$ mg m^{-2}; Cd: 0.05 ± 0.01 mg m^{-2}; Cr: 5.76 ± 1.31 mg m^{-2}), respectively. The Hg and Cr pool size in sea-buckthorn accounted for 84–100% and 81–100% of the total vegetation pool from the site 2010 to site 1995, respectively; while in fir accounted for 66–100% and 69–100% of the total vegetation pool from the 1963 site to 1926 site, respectively (Fig. S2). The Cd pool size in aspen accounted for 55–57% among the sites 1995–1963, and in fir accounted for 60–100% among the sites 1955–1926. The total Hg, Cd and Cr pool size in vegetation only accounted for 0.8%, 1.3% and 0.5% of total pool size (i.e., the sum of vegetation, Oi, Oe and 0–10 cm depth soils) across the whole deglacial forest chronosequence, respectively.

It is noted that we did not estimate soil pool sizes at 2010 site due to the soil mainly as the glacial moraine. The Hg pool sizes in Oi, Oe and 0–10 cm depth soils significantly increased with the glacial retreat time ($p < 0.05$), from 1.75 mg m^{-2} at 2005 site to 4.09 mg m^{-2} at 1926 site. The pool size of Cd in Oi, Oe and 0–10 cm depth soils showed the decreasing trends from 18.86 mg m^{-2} at 2005 site to 12.47 mg m^{-2} at

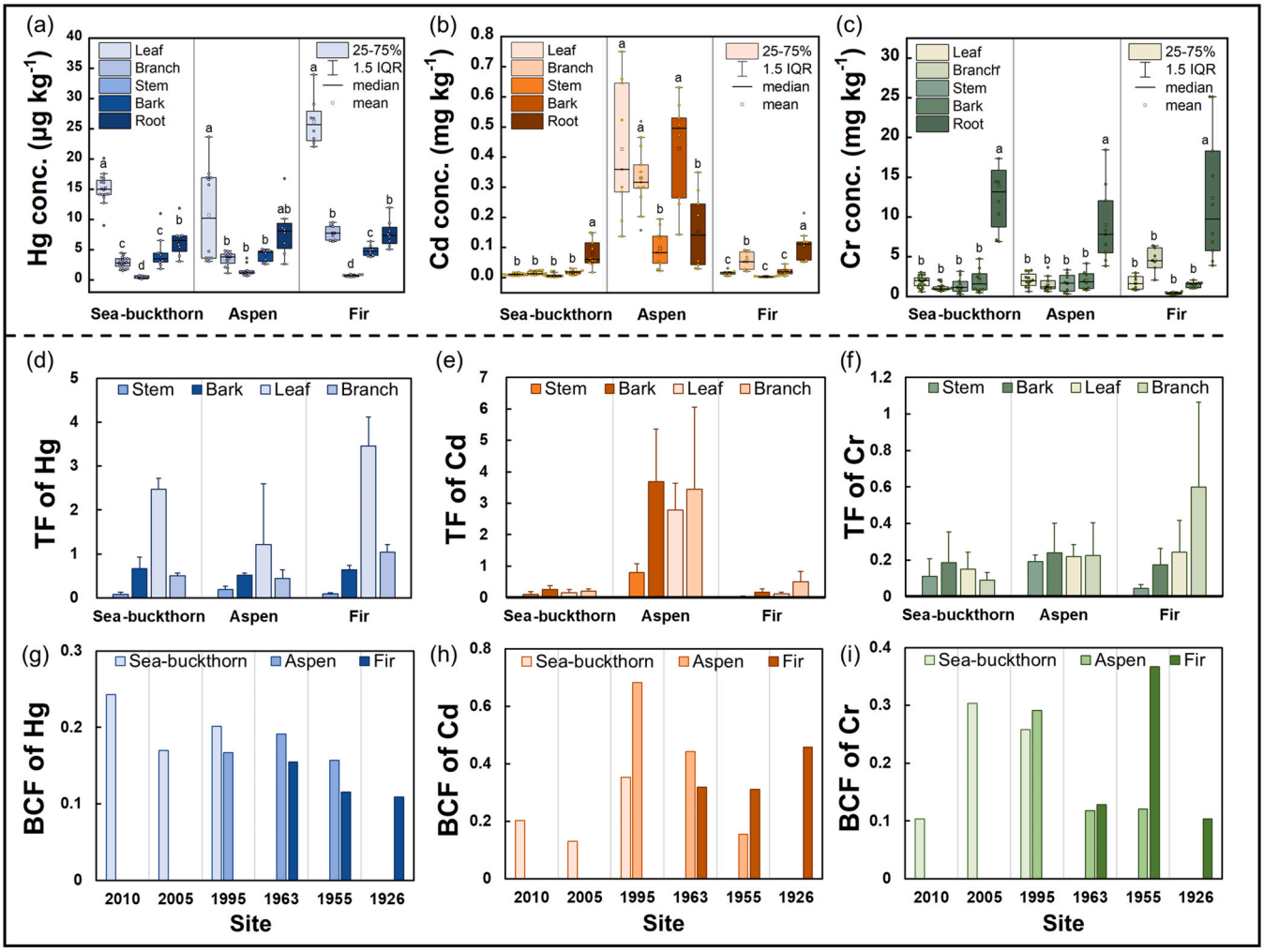

Fig. 3. (a-c) the concentration (conc.) of Hg, Cd and Cr; (d-f) the bioconcentration factor (BCF) of sea buckthorn, aspen and fir; (g-i) the translocation factor (TF) of sea buckthorn, aspen and fir in the forest chronosequence zone. IQR is the abbreviation of inter quartile range.

1955 site but then increased to 18.22 ± 1.50 mg m^{-2} at 1926 site. The Cr pool sizes in Oi, Oe and 0–10 cm depth soils decreased significantly with the glacier retreat from 5084.33 ± 410.27 mg m^{-2} at 2005 site to 2303.52 ± 365.92 mg m^{-2} at 1955 site, but then increased to 2538.53 ± 338.30 mg m^{-2} in the climax community of fir at 1926 site. Specially, Cr pool size of Oe decreased rapidly from 95.03 ± 1.04 mg m^{-2} at 1963 site to 25.62 ± 10.06 mg m^{-2} at 1955 site.

4. Discussion

4.1. Source estimation in soils

The almost constant values of Cd (0.29–0.38 mg kg^{-1}) and Cr concentrations (83.57–99.23 mg kg^{-1}) in C soil across the whole forest chronosequence (Fig. 2b-c) suggests that vegetation succession could pose a negligible effect on Cd and Cr concentration in deep soil horizons. The highest abundance of Cr in C soil and the low EF values of Cr (Fig. 2l) in topsoil indicate that weathering of moraine might be the main source of Cr [7]. Given the SOM is derived from the litter decomposition, the significantly negative correlation of Cr and SOM and positive correlation between pH and Cr (Fig. 2f and i) further support the importance of geogenic Cr inputs. The strong correlations among pH, SOM and Hg in topsoil (Fig. 2d and g) and the high EF values of Hg in topsoil (Fig. 2j) likely suggest the atmospheric Hg depositions as the main cause for topsoil Hg accumulation [93]. There are insignificant correlations of Cd to SOM and pH (Fig. 2e and h), possibly attributed to the mixing effects of geogenic sources (i.e., moraine weathering) and atmospheric depositions. Since the increase in soil organic matter leads to an increase in humic acids, which in turn leads to a decrease in pH. Therefore, the correlation between heavy metals and pH reflects the effect of vegetation succession on accumulation of heavy metals.

Furthermore, we used the PMF model to quantify contributions of atmospheric deposition and geogenic sources for Hg, Cd and Cr accumulation in topsoil. Modeling results of Oi-Oe (Fig. 5a) showed that Factor 1 had relatively high loading values for Cr, Be, Co and Ni (> 50%). Modeling results of 0–10 cm depth soils (Fig. 5b) also showed that Factor 1 had relatively high loading values for Cr, As, Pb, Li, Be, V, Mn, Co, Ni, Ga, Rb, Ag, Cs, Ba, Tl and U (> 70%). Since previous studies have well documented that Li, Be, V, Co, Ni, Ga, Cs and Ba are primarily derived from the crust of earth [33,46,81], Factor 1 in Oi-Oe and 0–10 cm depth soil mainly represents contribution of the geological sources. Modeling results showed that Factor 2 in Oi-Oe had relatively high loading values for Hg, As and Pb (> 46%), and 0–10 cm depth soils had the high loading of Hg (74%). The source contributions of Zn and Cd in Factor 3 of Oi-Oe were 65% and 56%, and source contribution of Zn in Factor 3 of 0–10 cm depth soils was 84%. Noteworthily, Hg, Zn, Cd, As and Pb are all susceptible to human activities [47,58,81,85] and atmospheric depositions are the dominant cause for their elevated accumulation in remote topsoil [115,18,22]. Atmospheric transportation and deposition of Zn and Cd are dominated by aerosol physiological

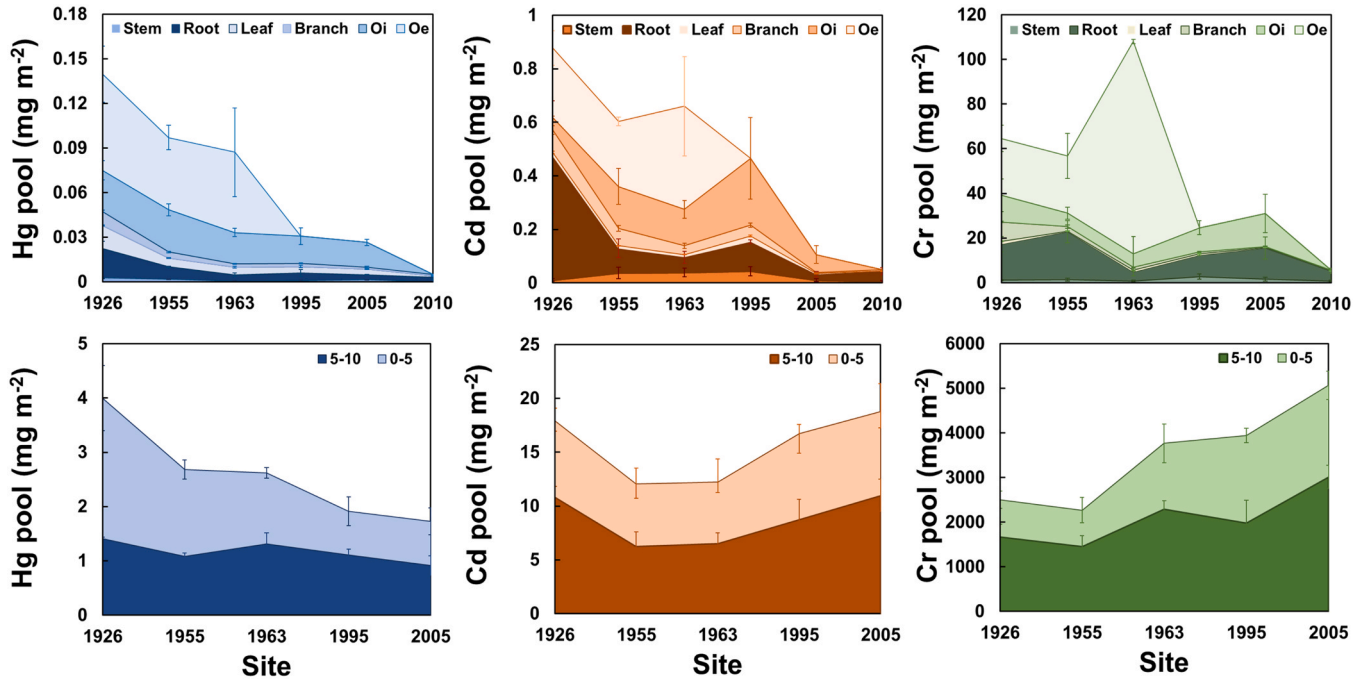

Fig. 4. Variations of pool sizes of Hg, Cd and Cr in vegetation biomass and soil profiles across the deglaciated forest chronosequence.

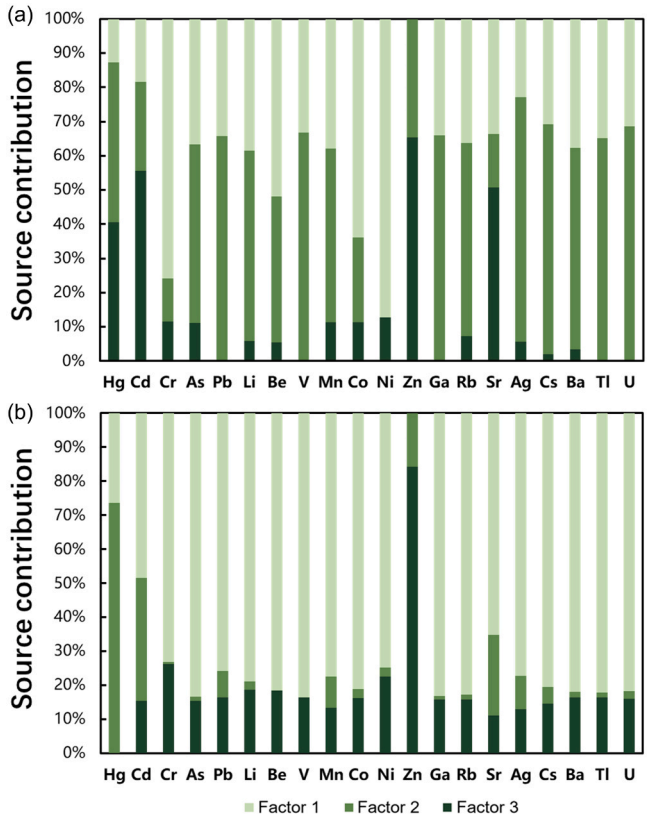

Fig. 5. Contributions of heavy metal sources by PMF model. (a) is for Oi and Oe; (b) is for 0–10 cm depth soils of the deglaciated forest chronosequence.

chemistry [107,12,63,93], while gaseous Hg^0 dry deposition as the main source of Hg in topsoil [91,36,52,92]. Therefore, both Factor 2 and Factor 3 represent impacts of anthropogenic emissions of HMs and the following atmospheric depositions.

From the summary of the PMF modeling results (Table S5), the atmospheric Hg deposition dominantly contributed to the Hg sources in topsoil (atmospheric Hg input in Oi-Oe: 87%; in 0–10 cm depth soils: 74%), whereas moraine weathering mostly contributed to the Cr sources in topsoil (Oi-Oe: 76%; 0–10 cm depth soils: 73%). Both moraine erosion (Oi-Oe: 18%; 0–10 cm depth soils: 48%) and atmospheric deposition (Oi-Oe: 82%; 0–10 cm depth soils: 52%) affected the Cd accumulation in topsoil.

4.2. *Heavy metals accumulation in plants*

Earlier studies have well documented that more than 90% of foliar Hg derived from the atmospheric Hg^0 [14,43]. Foliage takes up atmospheric Hg^0 mainly through the pathway of stomatal and non-stomatal (i.e., the adsorption of cuticle) [91,3,75]. After uptake, Hg is stored in foliage as complexes formed with reduced sulfur functional groups (Hg-SR), bis-thiolate complex ($Hg(SR)_2$) and Hg sulfide nanoparticles (β-HgS), and then migrates to other plant components through the sieve tube and xylem ray cells [97,95,3]. Therefore, the atmospheric Hg^0 uptake by foliage contributes to the main Hg sources in aboveground biomass ([91,37,52]; Zhou et al., 2021a; [117]). This is the reason for the elevated Hg concentration in foliage in contrast to Hg concentration in other tree components. Coniferous tree species have higher leaf Hg concentrations than deciduous tree species (Fig. 3). This is because much higher lifespan (3- to 5- year) of coniferous foliage leads to long-term of its foliage exposure into atmospheric Hg^0, when compared to 4 – 6 months of lifespan for deciduous foliage [91,116,117,39]. Additionally, the relatively high Hg concentration in root is attributed to the uptake of Hg (II) in soil solution by fine root [111,84]. The Hg isotopic signatures have suggested that the root uptake Hg was mainly fixed in epiblem, and hardly translocated into aboveground biomass [111].

Cd in vegetation mainly comes from soil Cd^{2+} uptake by roots [74]. Therefore, roots of sea buckthorn and fir have the elevated Cd concentrations. Cd^{2+} can be adsorbed on the surface of root epidermal cells and enter the root epidermal layer through the apoplast pathway [103,23,80], and also enter into plant cells through the ion channels of Fe^{2+}, Zn^{2+} and Ca^{2+} due to Cd^{2+} properties similar to these essential elements [2,45,65]. In addition, Cd^{2+} can form the metal-ligand complexes which with low molecular compounds secreted by roots, and enters the root

epidermis in the form of chelates [15]. Interestingly, the aboveground biomass of aspen has 1 – 2 times of Cd concentration than in roots (Fig. 3). This is because substantial Cd in root can be transported to aboveground biomass of aspen through ion channels with the assistance of translocators [106,73]. Specifically, the aspen foliage and bark are rich in terpenoids, suberin, fatty acid esters and amino acids which distinctly enhancing Cd translocation from roots to aboveground biomass [38,64].

Similarly, Cr in plants mainly derived from soil Cr uptake by roots. Cr in root can migrate into the aboveground biomass through the xylem vessel [28,87]. Compared to Hg and Cd, Cr is the least mobile in roots [69,71], due to the distinct root barrier against the Cr mobilization [62,70,72]. Therefore, we mainly observed the distinct Cr concentrations in roots of three tree species (Fig. 3).

The BCF values of Hg, Cd and Cr were less than 1 in the three tree species, implying the low accumulation of soil Hg, Cd and Cr in roots. Since Hg in plants mainly derived from the uptake of atmospheric Hg^0 by foliage, we would not discuss its TF values in vegetation. It is noted that the high TF values of Cd and Cr in bark of deciduous tree species cannot solely be explained by the root translocation. This is because the rough and porous structure of bark is beneficial to directly capture HMs from the atmosphere, thus also contributing to the elevated TF of Cd and Cr in the bark [54,55,5,79]. The smallest concentrations and TF values of Cd and Cr in most stem of tree species can be attribute to that the stem does not absorb metals directly due to stem mainly composed of cellulose, hemicellulose and lignin, and with the distinct biomass dilution caused by rapid xylem growth [25,34].

4.3. Accumulation variations during vegetation succession

The vegetation biomass production rapidly increased 1–2 times from 1955 site to 1926 site (Fig. S3) because of the competitive strategy of tree species that the greater woody mass competing more favorably [104]. At the site of 1926, the elevated pool sizes of Hg, Cd and Cr in vegetation were caused by the high vegetation biomass. The relatively high Cd pool size in vegetation at 1995 site was due to the elevated Cd accumulation in the aspen, which as the dominant tree species at this site.

As previously discussed, the atmospheric Hg^0 depositions are the main source for Hg accumulation in deglaciated forest soils [91,36,52,92]. Along with the vegetation succession, the increasing forest litter and SOM in topsoil would strongly promote the Hg accumulation in topsoil. At 2005 – 1963 sites, the litter and coarse woody debris with low Cd concentrations reduced the geologic Cd contribution. Thus, we observed a decreasing Cd pool of topsoil (Fig. 4). From 1955–1926 site, the litter decomposition of aspen with high Cd concentration (Fig. 3b) and the increasing atmospheric Cd depositions hereby lead to the elevated Cd pool sizes at these sites (Fig. 4). The geological inputs were as the major source of Cr in the deglaciated forest chronosequence, and the organic matters and woody biomass both have the relatively low Cr concentrations (Fig. 3). Therefore, the formation of organic matters in topsoil would decrease its Cr pool size [105].

To better understand accumulation variations of Hg, Cd and Cr along with the vegetation succession, we estimated the relative accumulation rates for Hg, Cd and Cr over the deglacial forest chronosequence by combining the pool sizes of vegetation, Oi, Oe and 0–10 cm depth soil profile. The relative heavy metal accumulation rate (Q_i, mg m^{-2} yr^{-1}) was estimated as following:

$$Q_i=(S_i-S_{(i-1)}) / \text{time} \quad (6)$$

where S is the total elemental pool size in topsoil (mg m^{-2}), and i denotes the pool size over a specified chronosequence, and time is the interval of glacial retreat time between two sites (year).

If atmospheric depositions are comparable among the deglaciated forest chronosequence, Q_i in the Eq. (6) would reflect changes of atmospheric heavy metal depositions over the past century. The historical trends of atmospheric Hg, Cd and Cr depositions have been well documented that the continuingly increasing depositions since 1850 s [6,13,48–50,57,68,77,90,101]. However, the accumulation rate of Hg showed a decreasing trend from 0.05 ± 0.01 mg m^{-2} yr^{-1} in 1920 s to 0.02 ± 0.00 mg m^{-2} yr^{-1} in 2000 s (Fig. 6). The accumulation rate of Cd also decreased from 0.21 ± 0.02 mg m^{-2} yr^{-1} in 1920 s to – 0.17 ± 0.09 mg m^{-2} yr^{-1} in 2000 s. The accumulation rate of Cr was 8.17 ± 0.95 mg m^{-2} yr^{-1} in 1920 s, and then showed the negative values from 1950 s to 2000 s, up to – 193.66 ± 13.20 mg m^{-2} yr^{-1} in 1960 s.

The discrepancy between accumulation rates and proposed atmospheric depositions can be attributed to impacts of increasing vegetation cover in the deglaciated forest chronosequence. As discussed, the vegetation succession would increase Hg and Cd accumulation in topsoil, while buffer the high Cr concentration of geogenic sources. Substantial glacial moraine mixed into the soil samples at 1963 site results in the elevated Cr pool size in Oe and 0–10 cm depth soils and as well as the lowest accumulation rates of Hg and Cr in 1960 s. The canopy of coniferous tree species could induce elevated atmospheric Hg, Cd and Cr depositions than of deciduous tree species because of larger interception of coniferous canopy [104,78]. Therefore, the accumulation rates of Hg, Cd and Cr were highest in coniferous forest. It is noted that the runoff and soil leaching processes in the forest floor would also lead to the Hg, Cd and Cr loss across the deglaciated forest chronosequence, specifically soil pH gradually changing from alkaline to acidic along with the vegetation succession (Fig. S4). The Hg, Cd and Cr loss rates in the coniferous forest could be slower than rates in the deciduous forests due to the coniferous hard-degraded substances (e.g., humin and lignin of needles) increasing the residence time of Hg, Cd and Cr in surface soil [11,4].

5. Conclusion

Our study shows that the vegetation succession in the deglaciated region significantly shapes the distribution, accumulation and allocation of Hg, Cd and Cr in the topsoil and vegetation. The atmospheric Hg^0 deposition is the main sources for Hg accumulation in topsoil, and the

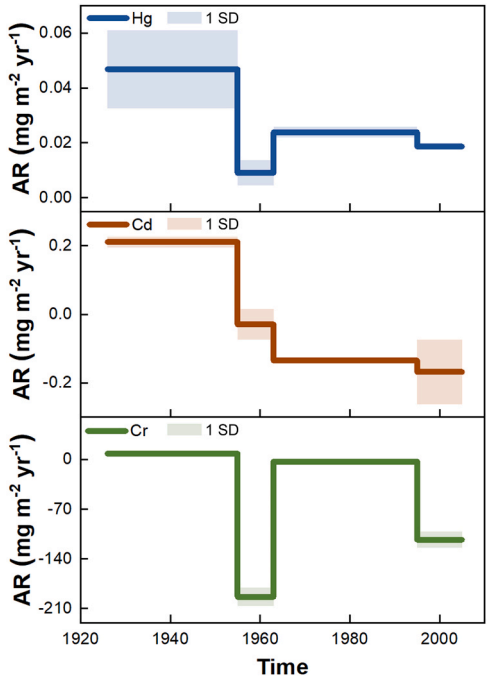

Fig. 6. Variations of accumulation rates (AR) of Hg, Cd and Cr (vegetation, Oi, Oe and 0–10 cm depth) across the deglaciated forest chronosequence.

Hg accumulation rate increases along with the pioneer deciduous forest to the climax coniferous forest stands. On the contrary, Cr is primarily derived from geological processes, the decreasing of geogenic Cr contribution in topsoil due to the increasing organic matter contents. Cd is enriched in topsoil and the main source of Cd shifts from the moraine weathering processes to atmospheric depositions along with the vegetation succession. Absorption and translocation of Hg, Cd and Cr in plants are distinctly different. Hg in plants is mainly from the uptake of atmospheric Hg^0 by foliage, while Cd and Cr in plants are predominantly from uptake by root. Our study indicates that vegetation succession contributes to the different biogeochemical processes of Hg, Cd and Cr among deglaciated forest chronosequence.

In this study, we used the statistical models to identify source contributions for each heavy metals. These statistical models are associated with uncertainties and cannot solely provide strongly direct evidence for quantification of source contributions. We recommend further studies to use the more direct and useful tools, such as isotopic signatures which have been identified to provide a new sight in source quantification [91, 96,110,111].

Furthermore, reforestation such as China's ecological restoration projects has significantly changed land covers across the globe [102,24, 53]. Our study provides an interesting sight in understanding the accumulation and transportation of HMs after the reforestation. Finally, identifying the potential threats to environment is critical, specifically under the contest of combined effects from anthropogenic influence and vegetation changes [82]. Thus, we recommend further studies focusing on the difference of their ecological risks of Hg, Cd and Cr in various vegetation successions.

CRediT authorship contribution statement

Peijia Chen: Sampling and Laboratory analysis, Conceptualization, Writing – original draft, Operation, Data curation, Software and Visualization. **Xun Wang, Wei Yuan** and **Dingyong Wang:** Conceptualization, Supervision, Writing – reviewing and editing. All authors have approval to the final version of the manuscript.

Declaration of Competing Interest

The authors declare that they have no known competing financial interests or personal relationships that could have appeared to influence the work reported in this paper.

Data availability

Data will be made available on request.

Acknowledgments

This work was funded by National Natural Science Foundation of China (41977272 and 42007307).

Appendix A. Supporting information

Supplementary data associated with this article can be found in the online version at doi:10.1016/j.jhazmat.2023.132162.

References

[1] Abrahim, G.M.S., Parker, R.J., 2008. Assessment of heavy metal enrichment factors and the degree of contamination in marine sediments from Tamaki Estuary, Auckland, New Zealand. Environ Monit Assess 136 (1), 227–238. https://doi.org/10.1007/s10661-007-9678-2.

[2] Ahmad, P., Sarwat, M., Bhat, N.A., Wani, M.R., Kazi, A.G., Tran, L.S., 2015. Alleviation of cadmium toxicity in Brassica juncea L.(Czern. & Coss.) by calcium application involves various physiological and biochemical strategies. PLoS One 10 (1), e0114571.

[3] Arnold, J., Gustin, M.S., Weisberg, P.J., 2018. Evidence for Nonstomatal Uptake of Hg by Aspen and Translocation of Hg from Foliage to Tree Rings in Austrian Pine. Environ Sci Technol 52 (3), 1174–1182. https://doi.org/10.1021/acs.est.7b04468.

[4] Berg, B., 2014. Decomposition patterns for foliar litter – A theory for influencing factors. Soil Biol Biochem 78, 222–232. https://doi.org/10.1016/j.soilbio.2014.08.005.

[5] Berlizov, A.N., Blum, O.B., Filby, R.H., Malyuk, I.A., Tryshyn, V.V., 2007. Testing applicability of black poplar (Populus nigra L.) bark to heavy metal air pollution monitoring in urban and industrial regions. Sci Total Environ 372 (2), 693–706. https://doi.org/10.1016/j.scitotenv.2006.10.029.

[6] BGS., 2019. *World mineral statistics data*. Retrieved from ⟨https://www.bgs.ac.uk/mineralsuk/statistics/home.html⟩:

[7] Bing, H., Wu, Y., Zhou, J., Li, R., Luo, J., Yu, D., 2016. Vegetation and cold trapping modulating elevation-dependent distribution of trace metals in soils of a high mountain in eastern Tibetan Plateau. Sci Rep 6, 24081. https://doi.org/10.1038/srep24081.

[8] Bing, H., Zhou, J., Wu, Y., Luo, X., Xiang, Z., Sun, H., Wang, J., Zhu, H., 2018. Barrier effects of remote high mountain on atmospheric metal transport in the eastern Tibetan Plateau. Sci Total Environ 628–629, 687–696. https://doi.org/10.1016/j.scitotenv.2018.02.035.

[9] Boutron, C.F., 1995. Historical reconstruction of the earth's past atmospheric environment from Greenland and Antarctic snow and ice cores. Environ Rev 3 (1), 1–28. https://doi.org/10.1139/a95-001.

[10] Brun, F., Berthier, E., Wagnon, P., Kääb, A., Treichler, D., 2017. A spatially resolved estimate of High Mountain Asia glacier mass balances from 2000 to 2016. Nat Geosci 10 (9), 668–673. https://doi.org/10.1038/ngeo2999.

[11] Chen, G., Fu, W., Lou, Y., Gao, W., Li, S., Yang, H., 2014. Effects of nitrogen addition on available nitrogen content and acidification in cold-temperate coniferous forest soil in the growing season. Environ Sci 35 (12), 4686–4694. https://doi.org/10.13227/j.hjkx.2014.12.036.

[12] Chueinta, W., Hopke, P.K., Paatero, P., 2000. Investigation of sources of atmospheric aerosol at urban and suburban residential areas in Thailand by positive matrix factorization. Atmos Environ 34 (20), 3319–3329. https://doi.org/10.1016/S1352-2310(99)00433-1.

[13] Cooke, C.A., Balcom, P.H., Biester, H., Wolfe, A.P., 2009. Over three millennia of mercury pollution in the Peruvian Andes. Proc Natl Acad Sci 106 (22), 8830–8834. https://doi.org/10.1073/pnas.0900517106.

[14] Cui, L., Feng, X., Lin, C.-J., Wang, X., Meng, B., Wang, X., Wang, H., 2014. Accumulation and translocation of 198Hg in four crop species. Environ Toxicol Chem 33 (2), 334–340. https://doi.org/10.1002/etc.2443.

[15] Curie, C., Cassin, G., Couch, D., Divol, F., Higuchi, K., Le Jean, M., Misson, J., Schikora, A., Czernic, P., Mari, S., 2009. Metal movement within the plant: contribution of nicotianamine and yellow stripe 1-like transporters. Ann Bot 103 (1), 1–11. https://doi.org/10.1093/aob/mcn207.

[16] Dong, Z., Kang, S., Qin, X., Li, X., Qin, D., Ren, J., 2015. New insights into trace elements deposition in the snow packs at remote alpine glaciers in the northern Tibetan Plateau, China. Sci Total Environ 529, 101–113. https://doi.org/10.1016/j.scitotenv.2015.05.065.

[17] Dragović, S., Mihailović, N., Gajić, B., 2008. Heavy metals in soils: Distribution, relationship with soil characteristics and radionuclides and multivariate assessment of contamination sources. Chemosphere 72 (3), 491–495. https://doi.org/10.1016/j.chemosphere.2008.02.063.

[18] Duan, Q., Lee, J., Liu, Y., Chen, H., Hu, H., 2016. Distribution of heavy metal pollution in surface soil samples in China: a graphical review. Bull Environ Contam Toxicol 97 (3), 303–309. https://doi.org/10.1007/s00128-016-1857-9.

[19] Edelstein, M., Ben-Hur, M., 2018. Heavy metals and metalloids: Sources, risks and strategies to reduce their accumulation in horticultural crops. Sci Hortic 234, 431–444. https://doi.org/10.1016/j.scienta.2017.12.039.

[20] EPA., 1982. *Intermedia Priority Pollutant Guidance Documents*. Retrieved from ⟨https://www.epa.gov⟩:

[21] Feng, X., Wang, X., Sun, G., Yuan, W., 2022. Research Progresses and Challenges of Mercury Biogeochemical Cycling in Global Vegetation Ecosystem. Earth Sci 47 (11), 4098–4107. https://doi.org/10.3799/dqkx.2022.882.

[22] Gautam, P.K., Gautam, R., Banerjee, S., Chattopadhyaya, M., & Pandey, J., 2016. Heavy metals in the environment: Fate, transport, toxicity and remediation technologies. In (pp. 101–130).

[23] Hans, B., 1990. Epidermal Uptake of Pb, Cd, and Zn in Tubificid Worms. Oecologia 85 (2), 226–232.

[24] Hua, F., Wang, X., Zheng, X., Fisher, B., Wang, L., Zhu, J., Wilcove, D.S., 2016. Opportunities for biodiversity gains under the world's largest reforestation programme. Nat Commun 7 (1), 12717. https://doi.org/10.1038/ncomms12717.

[25] Huang, F., Singh, P.M., Ragauskas, A.J., 2011. Characterization of Milled Wood Lignin (MWL) in Loblolly Pine Stem Wood, Residue, and Bark. J Agric Food Chem 59 (24), 12910–12916. https://doi.org/10.1021/jf202701b.

[26] Huang, J., Kang, S., Yin, R., Guo, J., Lepak, R., Mika, S., Tripathee, L., Sun, S., 2020. Mercury isotopes in frozen soils reveal transboundary atmospheric mercury deposition over the Himalayas and Tibetan Plateau. Environ Pollut 256, 113432. https://doi.org/10.1016/j.envpol.2019.113432.

[27] Jiao, X., Dong, Z., Kang, S., Li, Y., Jiang, C., Rostami, M., 2021. New insights into heavy metal elements deposition in the snowpacks of mountain glaciers in the eastern Tibetan Plateau. Ecotoxicol Environ Saf 207, 111228. https://doi.org/10.1016/j.ecoenv.2020.111228.

[28] Juneja, S., Prakash, S., 2005. The chemical form of trivalent chromium in xylem sap of maize (Zea mays L.). Chem Speciat Bioavailab 17 (4), 161–169. https://doi.org/10.3184/095422906783438820.

[29] Kaal, J., Perez-Rodriguez, M., Biester, H., 2022. Molecular Probing of DOM Indicates a Key Role of Spruce-Derived Lignin in the DOM and Metal Cycles of a Headwater Catchment: Can Spruce Forest Dieback Exacerbate Future Trends in the Browning of Central European Surface Waters? Environ Sci Technol 56 (4), 2747–2759. https://doi.org/10.1021/acs.est.1c04719.
[30] Kalavrouziotis, I., Rezapour, S., Koukoulakis, P.H., 2013. Wastewater status in Greece and Iran. Fresenius Environ Bull 22, 11–21.
[31] Kelly, J., Thornton, I., Simpson, P.R., 1996. Urban geochemistry: a study of the influence of anthropogenic activity on the heavy metal content of soils in traditionally industrial and non-industrial areas of Britain. Appl Geochem 11 (1), 363–370. https://doi.org/10.1016/0883-2927(95)00084-4.
[32] Kramer, M.G., Chadwick, O.A., 2018. Climate-driven thresholds in reactive mineral retention of soil carbon at the global scale. Nat Clim Change 8 (12), 1104–1108. https://doi.org/10.1038/s41558-018-0341-4.
[33] Li, C., Zhou, K., Qin, W., Tian, C., Qi, M., Yan, X., Han, W., 2019. A review on heavy metals contamination in soil: effects, sources, and remediation techniques. Soil Sediment Contam: Int J 28 (4), 380–394. https://doi.org/10.1080/15320383.2019.1592108.
[34] Li, J., He, Y., Duan, J., Zhang, Q., 2012. Absorption and Accumulation of Heavy Metal from Soil by Leaves of Populus × euramericana cv. 'Neva' Plantation. Res 25 (01), 65–70. https://doi.org/10.13275/j.cnki.lykxyj.2012.01.001.
[35] Li, X., Sun, G., Chen, S., Fang, Z., Yuan, H., Shi, Q., Zhu, Y., 2018. Molecular chemodiversity of dissolved organic matter in paddy soils. Environ Sci Technol 52 (3), 963–971. https://doi.org/10.1021/acs.est.7b00377.
[36] Lindberg, S., Bullock, R., Ebinghaus, R., Engstrom, D., Feng, X., Fitzgerald, W., Pirrone, N., Prestbo, E., Seigneur, C., 2007. A synthesis of progress and uncertainties in attributing the sources of mercury in deposition. Ambio 36 (1), 19–32 doi:10.1579/0044-7447(2007)36[19:asopau]2.0.co;2.
[37] Liu, N., Cai, X., Jia, L., Wang, X., Yuan, W., Lin, C.-J., Wang, D., Feng, X., 2023. Quantifying mercury distribution and source contribution in surface soil of qinghai-tibetan plateau using mercury isotopes. Environ Sci Technol. https://doi.org/10.1021/acs.est.2c09610.
[38] Liu, X., Peng, K., Wang, A., Lian, C., Shen, Z., 2010. Cadmium accumulation and distribution in populations of Phytolacca americana L. and the role of transpiration. Chemosphere 78 (9), 1136–1141. https://doi.org/10.1016/j.chemosphere.2009.12.030.
[39] Liu, Y., Liu, G., Wang, Z., Guo, Y., Yin, Y., Zhang, X., Cai, Y., Jiang, G., 2022. Understanding foliar accumulation of atmospheric Hg in terrestrial vegetation: Progress and challenges. Crit Rev Environ Sci Technol 52 (24), 4331–4352. https://doi.org/10.1080/10643389.2021.1989235.
[40] Luo, X., Yu, S., Zhu, Y., Li, X., 2012. Trace metal contamination in urban soils of China. Sci Total Environ 421–422, 17–30. https://doi.org/10.1016/j.scitotenv.2011.04.020.
[41] Lv, J., Zhang, S., Wang, S., Luo, L., Cao, D., Christie, P., 2016. Molecular-Scale Investigation with ESI-FT-ICR-MS on Fractionation of Dissolved Organic Matter Induced by Adsorption on Iron Oxyhydroxides. Environ Sci Technol 50 (5), 2328–2336. https://doi.org/10.1021/acs.est.5b04996.
[42] Magnani, A., Ajmone-Marsan, F., D'Amico, M., Balestrini, R., Viviano, G., Salerno, F., Freppaz, M., 2018. Soil properties and trace elements distribution along an altitudinal gradient on the southern slope of Mt. Everest, Nepal. Catena 162, 61–71. https://doi.org/10.1016/j.catena.2017.11.015.
[43] Mao, Y., Li, Y., Richards, J., Cai, Y., 2013. Investigating uptake and translocation of mercury species by Sawgrass (Cladium jamaicense) using a stable isotope tracer technique. Environ Sci Technol 47 (17), 9678–9684. https://doi.org/10.1021/es400546s.
[44] McConnell, J.R., Edwards, R., 2008. Coal burning leaves toxic heavy metal legacy in the Arctic. Proc Natl Acad Sci 105 (34), 12140–12144. https://doi.org/10.1073/pnas.0803564105.
[45] Murtaza, G., Javed, W., Hussain, A., Qadir, M., Aslam, M., 2017. Soil-applied zinc and copper suppress cadmium uptake and improve the performance of cereals and legumes. Int J Phytoremediat 19 (2), 199–206. https://doi.org/10.1080/15226514.2016.1207605.
[46] Nagajyoti, P.C., Lee, K.D., Sreekanth, T.V.M., 2010. Heavy metals, occurrence and toxicity for plants: a review. Environ Chem Lett 8 (3), 199–216. https://doi.org/10.1007/s10311-010-0297-8.
[47] Naila, A., Meerdink, G., Jayasena, V., Sulaiman, A.Z., Ajit, A.B., Berta, G., 2019. A review on global metal accumulators—mechanism, enhancement, commercial application, and research trend. Environ Sci Pollut Res 26 (26), 26449–26471. https://doi.org/10.1007/s11356-019-05992-4.
[48] Ni, R., Ma, Y., 2018. Current inventory and changes of the input/output balance of trace elements in farmland across China. PLoS One 13 (6), e0199460. https://doi.org/10.1371/journal.pone.0199460.
[49] Norton, S.A., Wilson, T., Handley, M., Osterberg, E.C., 2007. Atmospheric deposition of cadmium in the northeastern USA. Appl Geochem 22 (6), 1217–1222. https://doi.org/10.1016/j.apgeochem.2007.03.014.
[50] Nriagu, J.O., 1979. Global inventory of natural and anthropogenic emissions of trace metals to the atmosphere. Nature 279 (5712), 409–411. https://doi.org/10.1038/279409a0.
[51] Nriagu, J.O., 1996. A history of global metal pollution. -223 Science 272 (5259), 223. https://doi.org/10.1126/science.272.5259.223.
[52] Obrist, D., Kirk, J.L., Zhang, L., Sunderland, E.M., Jiskra, M., Selin, N.E., 2018. A review of global environmental mercury processes in response to human and natural perturbations: Changes of emissions, climate, and land use. Ambio 47 (2), 116–140. https://doi.org/10.1007/s13280-017-1004-9.
[53] Ouyang, Z., Zheng, H., Xiao, Y., Polasky, S., Liu, J., Xu, W., Daily, G.C., 2016. Improvements in ecosystem services from investments in natural capital. Science 352 (6292), 1455–1459. https://doi.org/10.1126/science.aaf2295.
[54] Pacheco, A.M.G., Barros, L.I.C., Freitas, M.C., Reis, M.A., Hipólito, C., Oliveira, O. R., 2002. An evaluation of olive-tree bark for the biological monitoring of airborne trace-elements at ground level. Environ Pollut 120 (1), 79–86. https://doi.org/10.1016/S0269-7491(02)00130-6.
[55] Patrick, G.J., Farmer, J.G., 2007. A lead isotopic assessment of tree bark as a biomonitor of contemporary atmospheric lead. Sci Total Environ 388 (1), 343–356. https://doi.org/10.1016/j.scitotenv.2007.07.047.
[56] Pecina, V., Valtera, M., Drapela, K., Novotny, R., Vahalik, P., Komendova, R., Brtnicky, M., Juricka, D., 2022. Influence of beech and spruce on potentially toxic elements-related health risk of edible mushrooms growing on unpolluted forest soils. Sci Rep 12 (1), 5407. https://doi.org/10.1038/s41598-022-09400-9.
[57] Peng, H., Chen, Y., Weng, L., Ma, J., Ma, Y., Li, Y., Islam, M.S., 2019. Comparisons of heavy metal input inventory in agricultural soils in North and South China: A review. Sci Total Environ 660, 776–786. https://doi.org/10.1016/j.scitotenv.2019.01.066.
[58] Qin, G., Niu, Z., Yu, J., Li, Z., Ma, J., Xiang, P., 2021. Soil heavy metal pollution and food safety in China: Effects, sources and removing technology. Chemosphere 267, 129205. https://doi.org/10.1016/j.chemosphere.2020.129205.
[59] Quantin, C., Ettler, V., Garnier, J., Šebek, O., 2008. Sources and extractibility of chromium and nickel in soil profiles developed on Czech serpentinites. Comptes Rendus Geosci 340 (12), 872–882. https://doi.org/10.1016/j.crte.2008.07.013.
[60] Ratering, S., Schnell, S., 2000. Localization of iron-reducing activity in paddy soilby profile studies. Biogeochemistry 48 (3), 341–365. https://doi.org/10.1023/A:1006252315427.
[61] Redondo-Gómez, S., Mateos-Naranjo, E., Andrades-Moreno, L., 2010. Accumulation and tolerance characteristics of cadmium in a halophytic Cd-hyperaccumulator, Arthrocnemum macrostachyum. J Hazard Mater 184 (1), 299–307. https://doi.org/10.1016/j.jhazmat.2010.08.036.
[62] Rezapour, S., Atashpaz, B., Moghaddam, S.S., Kalavrouziotis, I.K., Damalas, C.A., 2019. Cadmium accumulation, translocation factor, and health risk potential in a wastewater-irrigated soil-wheat (Triticum aestivum L.) system. Chemosphere 231, 579–587. https://doi.org/10.1016/j.chemosphere.2019.05.095.
[63] Rogge, W.F., Hildemann, L.M., Mazurek, M.A., Cass, G.R., Simoneit, B.R.T., 1993. Sources of fine organic aerosol. 3. Road dust, tire debris, and organometallic brake lining dust: roads as sources and sinks. Environ Sci Technol 27 (9), 1892–1904. https://doi.org/10.1021/es00046a019.
[64] Rong, G., Chu, Y., Liu, S., Kataweteetham, L., Zhu, J.J.B., 2021. Comparison of cadmium accumulation in upright and leaning poplar trees. BioResources 16 (2), 3422–3436.
[65] Sadana, U.S., Samal, D., Claassen, N., 2003. Differences in manganese efficiency of wheat (Triticum aestivum L.) and raya (Brassica juncea L.) as related to root-shoot relations and manganese influx. J Plant Nutr Soil Sci 166 (3), 385–389. https://doi.org/10.1002/jpln.200390059.
[66] Selin, N.E., 2009. Global biogeochemical cycling of mercury: a review. Annu Rev Environ Resour 34 (1), 43–63. https://doi.org/10.1146/annurev.environ.051308.084314.
[67] Serbula, S.M., Radojevic, A.A., Kalinovic, J.V., Kalinovic, T.S., 2014. Indication of airborne pollution by birch and spruce in the vicinity of copper smelter. Environ Sci Pollut Res 21 (19), 11510–11520. https://doi.org/10.1007/s11356-014-3120-4.
[68] Shahid, M., Shamshad, S., Rafiq, M., Khalid, S., Bibi, I., Niazi, N.K., Dumat, C., Rashid, M.I., 2017. Chromium speciation, bioavailability, uptake, toxicity and detoxification in soil-plant system: A review. Chemosphere 178, 513–533. https://doi.org/10.1016/j.chemosphere.2017.03.074.
[69] Shanker, A.K., Cervantes, C., Loza-Tavera, H., Avudainayagam, S., 2005. Chromium toxicity in plants. Environ Int 31 (5), 739–753. https://doi.org/10.1016/j.envint.2005.02.003.
[70] Shanker, A.K., Djanaguiraman, M., Sudhagar, R., Chandrashekar, C.N., Pathmanabhan, G., 2004. Differential antioxidative response of ascorbate glutathione pathway enzymes and metabolites to chromium speciation stress in green gram (Vigna radiata (L.) R.Wilczek. cv CO 4) roots. Plant Sci 166 (4), 1035–1043. https://doi.org/10.1016/j.plantsci.2003.12.015.
[71] Shukla, O.P., Dubey, S., Rai, U.N., 2007. Preferential accumulation of cadmium and chromium: toxicity in Bacopa monnieri L. under mixed metal treatments. Bull Environ Contam Toxicol 78 (3), 252–257. https://doi.org/10.1007/s00128-007-9155-1.
[72] Singh, H.P., Mahajan, P., Kaur, S., Batish, D.R., Kohli, R.K., 2013. Chromium toxicity and tolerance in plants. Environ Chem Lett 11 (3), 229–254. https://doi.org/10.1007/s10311-013-0407-5.
[73] Solti, Á., Sárvári, É., Tóth, B., Basa, B., Lévai, L., Fodor, F., 2011. Cd affects the translocation of some metals either Fe-like or Ca-like way in poplar. Plant Physiol Biochem 49 (5), 494–498. https://doi.org/10.1016/j.plaphy.2011.01.011.
[74] Song, Y., Jin, L., Wang, X., 2017. Cadmium absorption and transportation pathways in plants. Int J Phytoremediat 19 (2), 133–141. https://doi.org/10.1080/15226514.2016.1207598.
[75] Stamenkovic, J., Gustin, M.S., 2009. Nonstomatal versus stomatal uptake of atmospheric mercury. Environ Sci Technol 43 (5), 1367–1372. https://doi.org/10.1021/es801583a.
[76] Steve, L., Russell, B., Ralf, E., Daniel, E., Xinbin, F., William, F., Nicola, P., Eric, P., Christian, S., 2007. A synthesis of progress and uncertainties in attributing the sources of mercury in deposition. Ambio 36 (1), 19–33 doi:10.1579/0044-7447(2007)36[19:ASOPAU]2.0.CO;2.

[77] Streets, D.G., Zhang, Q., Wu, Y., 2009. Projections of global mercury emissions in 2050. Environ Sci Technol 43 (8), 2983–2988. https://doi.org/10.1021/es802474j.
[78] Sun, X., Wang, G., Wu, Y., Liu, L., Liu, G., 2013. Hydrologic regime of interception for typical forest ecosystem at subalpine of Western Sichuan, China. ACTA ECOLOGICA Sin 33 (02), 501–508. https://doi.org/10.5846/stxb201111301828.
[79] Świsłowski, P., Kříž, J., Rajfur, M., 2020. The use of bark in biomonitoring heavy metal pollution of forest areas on the example of selected areas in Poland. Ecol Chem Eng S 27 (2), 195–210. https://doi.org/10.2478/eces-2020-0013.
[80] Takahashi, R., Ishimaru, Y., Shimo, H., Ogo, Y., Senoura, T., Nishizawa, N.K., Nakanishi, H., 2012. The OsHMA2 transporter is involved in root-to-shoot translocation of Zn and Cd in rice. Plant, Cell Environ 35 (11), 1948–1957. https://doi.org/10.1111/j.1365-3040.2012.02527.x.
[81] Tchounwou, P.B., Yedjou, C.G., Patlolla, A.K., Sutton, D.J., 2012. Heavy Metal Toxicity and the Environment. In: Luch, A. (Ed.), Molecular, Clinical and Environmental Toxicology, Vol. 101. Springer Basel, Basel, pp. 133–164.
[82] Tong, X., Brandt, M., Yue, Y., Horion, S., Wang, K., Keersmaecker, W.D., Fensholt, R., 2018. Increased vegetation growth and carbon stock in China karst via ecological engineering. Nat Sustain 1 (1), 44–50. https://doi.org/10.1038/s41893-017-0004-x.
[83] Tóth, G., Hermann, T., Szatmári, G., Pásztor, L., 2016. Maps of heavy metals in the soils of the European Union and proposed priority areas for detailed assessment. Sci Total Environ 565, 1054–1062. https://doi.org/10.1016/j.scitotenv.2016.05.115.
[84] Trakal, L., Martínez-Fernández, D., Vítková, M., Komárek, M., 2015. Phytoextraction of Metals: Modeling Root Metal Uptake and Associated Processes. In: Ansari, A.A., Gill, S.S., Gill, R., Lanza, G.R., Newman, L. (Eds.), *Phytoremediation: Manag*ement of Env*i*ronmen*t*al C*ontamin*ant*s*, Volume 1. Springer International Publishing, Cham, pp. 69–83.
[85] Tyler, G., 1990. Bryophytes and heavy metals: a literature review. Bot J Linn Soc 104 (1–3), 231–253. https://doi.org/10.1111/j.1095-8339.1990.tb02220.x.
[86] Van de Velde, K., Ferrari, C., Barbante, C., Moret, I., Bellomi, T., Hong, S., Boutron, C., 1999. A 200 Year Record of Atmospheric Cobalt, Chromium, Molybdenum, and Antimony in High Altitude Alpine Firn and Ice. Environ Sci Technol 33 (20), 3495–3501. https://doi.org/10.1021/es990066y.
[87] Verma, S.J., Prakash, S., 2012. Studies on Cr (III) and Cr (VI) Speciation in the Xylem Sap of Maize Plants. In: Khemani, L.D., Srivastava, M.M., Srivastava, S. (Eds.), Chemistry of Phytopotentials: Health, Energy and Environmental Perspectives. Springer Berlin Heidelberg, Berlin, Heidelberg, pp. 269–274.
[88] Vitousek, P.M., Mooney, H.A., Lubchenco, J., Melillo, J.M., 1997. Human Domination of Earth's Ecosystems. Science 277 (5325), 494–499. https://doi.org/10.1126/science.277.5325.494.
[89] Walkley, A., 1947. A critical examination of a rapid method for determining organic carbon in soils—effect of variations in digestion conditions and of inorganic soil constituents. Soil Sci 63 (4).
[90] Wang, C., Liu, Y., Zhang, W., Hong, S., Hur, S.D., Lee, K., Pang, H., Hou, S., 2016. High-resolution atmospheric cadmium record for AD 1776–2004 in a high-altitude ice core from the eastern Tien Shan, central Asia. Ann Glaciol 57 (71), 265–272. https://doi.org/10.3189/2016AoG71A501.
[91] Wang, X., Yuan, W., Lin, C.-J., Feng, X., 2022. Mercury cycling and isotopic fractionation in global forests. Crit Rev Environ Sci Technol 52 (21), 3763–3786. https://doi.org/10.1080/10643389.2021.1961505.
[92] Wang, X., Bao, Z., Lin, C.-J., Yuan, W., Feng, X., 2016. Assessment of Global Mercury Deposition through Litterfall. Environ Sci Technol 50 (16), 8548–8557. https://doi.org/10.1021/acs.est.5b06351.
[93] Wang, X., Yuan, W., Feng, X., Wang, D., Luo, J., 2019. Moss facilitating mercury, lead and cadmium enhanced accumulation in organic soils over glacial erratic at Mt. Gongga, China. Environ Pollut 254 (Pt A), 112974. https://doi.org/10.1016/j.envpol.2019.112974.
[94] Wang, X., Luo, J., Lin, C.-J., Wang, D., Yuan, W., 2020. Elevated cadmium pollution since 1890s recorded by forest chronosequence in deglaciated region of Gongga, China. Environ Pollut 260, 114082. https://doi.org/10.1016/j.envpol.2020.114082.
[95] Wang, X., Yuan, W., Lin, C.-J., Wu, F., Feng, X., 2021. Stable mercury isotopes stored in Masson Pinus tree rings as atmospheric mercury archives. J Hazard Mater 415, 125678. https://doi.org/10.1016/j.jhazmat.2021.125678.
[96] Wang, X., Yuan, W., Lin, C.-J., Zhang, L., Zhang, H., Feng, X., 2019. Climate and Vegetation As Primary Drivers for Global Mercury Storage in Surface Soil. Environ Sci Technol 53 (18), 10665–10675. https://doi.org/10.1021/acs.est.9b02386.
[97] Wang, X., Yuan, W., Lin, C.-J., Luo, J., Wang, F., Feng, X., Fu, X., Liu, C., 2020. Underestimated Sink of Atmospheric Mercury in a Deglaciated Forest Chronosequence. Environ Sci Technol 54 (13), 8083–8093. https://doi.org/10.1021/acs.est.0c01667.
[98] Wang, X., Luo, J., Yuan, W., Lin, C.J., Wang, F., Liu, C., Wang, G., Feng, X., 2020. Global warming accelerates uptake of atmospheric mercury in regions experiencing glacier retreat. Proc Natl Acad Sci USA 117 (4), 2049–2055. https://doi.org/10.1073/pnas.1906930117.
[99] Wang, X., Luo, J., Yin, R., Yuan, W., Lin, C.-J., Sommar, J., Feng, X., Wang, H., Lin, C., 2017. Using mercury isotopes to understand mercury accumulation in the montane forest floor of the eastern Tibetan Plateau. Environ Sci Technol 51 (2), 801–809. https://doi.org/10.1021/acs.est.6b03806.
[100] Wu, R., Dong, Z., Cheng, X., Brahney, J., Jiao, X., & Wu, L., 2022. Heavy metal levels and sources in suspended particulate matters of the glacier watersheds in Northeast Tibetan Plateau. 10. doi:10.3389/fenvs.2022.918514.
[101] Wu, Y., Wang, S., Streets, D.G., Hao, J., Chan, M., Jiang, J., 2006. Trends in anthropogenic mercury emissions in China from 1995 to 2003. Environ Sci Technol 40 (17), 5312–5318. https://doi.org/10.1021/es060406x.
[102] Xu, W., Xiao, Y., Zhang, J., Yang, W., Zhang, L., Hull, V., Ouyang, Z., 2017. Strengthening protected areas for biodiversity and ecosystem services in China. Proc Natl Acad Sci 114 (7), 1601–1606. https://doi.org/10.1073/pnas.1620503114.
[103] Yamaguchi, N., Mori, S., Baba, K., Kaburagi-Yada, S., Arao, T., Kitajima, N., Hokura, A., Terada, Y., 2011. Cadmium distribution in the root tissues of solanaceous plants with contrasting root-to-shoot Cd translocation efficiencies. Environ Exp Bot 71 (2), 198–206. https://doi.org/10.1016/j.envexpbot.2010.12.002.
[104] Yang, D., Luo, J., She, J., Tang, R., 2015. Dynamics of Vegetation Biomass Along the Chronosequence in Hailuogou Glacier Retreated Area, Mt. Gongga. Ecol Environ Sci 24 (11), 1843–1850. https://doi.org/10.16258/j.cnki.1674-5906.2015.11.014.
[105] Yang, W., Zeng, X., Lv, Z., Liu, N., Chen, P., Wang, X., Wang, D., 2022. Distribution, accumulation and source of chromium in typical glacier retreated area of Tibetan Plateau: a case study of Hailuogou glacier retreated area. China Environ Sci 1–11. https://doi.org/10.19674/j.cnki.issn1000-6923.20220616.016.
[106] Yang, Y., Wang, G., 2017. Poplar Response to Cd Stress and Its Resistance Mechanism. World Res 30 (04), 29–34. https://doi.org/10.13348/j.cnki.sjlyyj.2017.0042.y.
[107] Yang, Y., Wang, Y., Wen, T., Li, W., Zhao, Y. n, Li, L., 2009. Elemental composition of PM2.5 and PM10 at Mount Gongga in China during 2006. Atmos Res 93 (4), 801–810. https://doi.org/10.1016/j.atmosres.2009.03.014.
[108] Yao, T., Thompson, L., Yang, W., Yu, W., Gao, Y., Guo, X., Yang, X., Duan, K., Zhao, H., Xu, B., Pu, J., Lu, A., Xiang, Y., Kattel, D., Joswiak, D., 2012. Different glacier status with atmospheric circulations in Tibetan Plateau and surroundings. Nat Clim Change 2 (9), 663–667. https://doi.org/10.1038/nclimate1580.
[109] Yu, S., Lv, J., Jiang, L., Geng, P., Cao, D., Wang, Y., 2023. Changes of soil dissolved organic matter and its relationship with microbial community along the hailuogou glacier forefield chronosequence. Environ Sci Technol 57 (9), 4027–4038. https://doi.org/10.1021/acs.est.2c08855.
[110] Yuan, W., Wang, X., Lin, C.-J., Sommar, J.O., Wang, B., Lu, Z., Feng, X., 2021. Quantification of atmospheric mercury deposition to and legacy re-emission from a subtropical forest floor by mercury isotopes. Environ Sci Technol 55 (18), 12352–12361. https://doi.org/10.1021/acs.est.1c02744.
[111] Yuan, W., Wang, X., Lin, C.-J., Wu, F., Luo, K., Zhang, H., Lu, Z., Feng, X., 2022. Mercury uptake, accumulation, and translocation in roots of subtropical forest: implications of global mercury budget. Environ Sci Technol 56 (19), 14154–14165. https://doi.org/10.1021/acs.est.2c04217.
[112] Zacchini, M., Pietrini, F., Scarascia Mugnozza, G., Iori, V., Pietrosanti, L., Massacci, A., 2009. Metal Tolerance, Accumulation and Translocation in Poplar and Willow Clones Treated with Cadmium in Hydroponics. Water, Air, Soil Pollut 197 (1), 23–34. https://doi.org/10.1007/s11270-008-9788-7.
[113] Zhang, X., Wu, J., Wang, C., HE, X., QI, Y., 2006. Vertical geomorphologic zonation in the northwest sichuan plateau and freezing planation surface. Mt Res 05, 607–611.
[114] Zheng, B., Zhao, X., Li, T., Wang, C., 1999. Features and fluctuation of the melang glacier in the mainri mountain. J Glaciology Geocryology 21 (02), 145–150.
[115] Zhong, T., Xue, D., Zhao, L., Zhang, X., 2018. Concentration of heavy metals in vegetables and potential health risk assessment in China. Environ Geochem Health 40 (1), 313–322. https://doi.org/10.1007/s10653-017-9909-6.
[116] Zhou, J., Obrist, D., 2021. Global mercury assimilation by vegetation. Environ Sci Technol 55 (20), 14245–14257. https://doi.org/10.1021/acs.est.1c03530.
[117] Zhou, J., Obrist, D., Dastoor, A., Jiskra, M., Ryjkov, A., 2021. Vegetation uptake of mercury and impacts on global cycling. Nat Rev Earth Environ 2 (4), 269–284. https://doi.org/10.1038/s43017-021-00146-y.
[118] Zhou, J., Wu, Y., Prietzel, J., Bing, H., Yu, D., Sun, S., Luo, J., Sun, H., 2013. Changes of soil phosphorus speciation along a 120-year soil chronosequence in the Hailuogou Glacier retreat area (Gongga Mountain, SW China). Geoderma 195–196, 251–259. https://doi.org/10.1016/j.geoderma.2012.12.010.
[119] Zhou, J., Du, B., Wang, Z., Zhang, W., Xu, L., Fan, X., Liu, X., Zhou, J., 2019. Distributions and pools of lead (Pb) in a terrestrial forest ecosystem with highly elevated atmospheric Pb deposition and ecological risks to insects. Sci Total Environ 647, 932–941. https://doi.org/10.1016/j.scitotenv.2018.08.091.